Applied Thermal Engineering 102 (2016) 1287–1299

Contents lists available at ScienceDirect

Applied Thermal Engineering

journal homepage: www.elsevier.com/locate/apthermeng

Research Paper

Thermo-mechanical analysis of double base propellant combustion in a barrel

Ercan Değirmenci [a], Celal Evci [b,*], Halil Işık [a], Mehmet Macar [a], Nadir Yılmaz [c], M. Hüsnü Dirikolu [d], Veli Çelik [e]

[a] Turkish Military Academy, Mechanical Engineering Department, Ankara, Turkey
[b] Turkish Military Academy, Defense Sciences Institute, Ankara, Turkey
[c] Department of Mechanical Engineering, New Mexico Institute of Mining and Technology, NM, USA
[d] Istanbul University, Mechanical Engineering Dept., Avcilar Kampus, Istanbul, Turkey
[e] Yıldırım Beyazıt University, Engineering and Natural Sciences Faculty, Ankara, Turkey

HIGHLIGHTS

- Propellant grain size and initial temperature alter the interior ballistic parameters.
- Numerical model of interior ballistics problem was validated experimentally.
- Developed thermo-mechanical model can be used for small and large caliber weapons.
- Heat transfer and stress analysis were done using numerical and analytical methods.
- Thermal effects and stresses determined the barrel behavior for successive shots.

ARTICLE INFO

Article history:
Received 4 January 2016
Accepted 14 April 2016

Keywords:
Burn rate
Thermo-mechanical modeling
Thermal stress
Stress analysis
Gun barrel
Experimental verification

ABSTRACT

Accurate determination of burning characteristics of the propellant and thermo-mechanical loads acting on the barrel supports better gun design and its tactical use. As the frequency of successive shots changes, burning rate of the gun propellant also changes and consequently the bullet velocity and internal pressure of the barrel changes as well. In this work, combustion characteristics of double base propellants with various grain sizes and initial temperatures were determined by performing a series of shooting tests and employing a thermo-mechanical model with ABAQUS® finite element code. Effects of various grain sizes (300–425, 425–500, 500–600, 600–710, 710–850 μm) and initial temperatures (−60, −20, 0, 20, and 60 °C) of double base propellants on internal pressure, bullet velocity and barrel heat transfer were investigated experimentally and computationally. Samples of propellants were tested in a shooting range by using a NATO standard small caliber barrel of 7.62 mm in diameter, and barrel internal pressure, bullet velocity and barrel surface temperatures were measured experimentally. The barrel experienced high thermal stresses during the shootings. Based on the comparisons between the simulations and the experiments, the finite element model was in agreement with the data within 90% accuracy.

© 2016 Elsevier Ltd. All rights reserved.

1. Introduction

The analysis of propellant combustion and thermo-mechanical loading generated inside the barrel along with the projectile motion through the barrel is the subject matter of interior ballistics. Many physical and chemical approaches are employed to improve the interior ballistic performance of guns with consideration based on the relationship between the gas pressure and projectile velocity. Because of the high degree of nonlinearity of combustion and the variables basic to the problem such as chemical composition of the propellant, rate of reaction, ignition characteristics, grain geometry, grain size, charge weight and environmental factors solution of the interior ballistic problem is not simple [1]. The solution may be based on theoretical analysis, established empirical relationships, numerical methods and detailed experimentation.

Bullets that are used in a barrel with helical grooves receive their energy inside the barrel from a gun propellant and keep their projectile path without any external correction until reaching their targets. Gun propellants burn without any need for an oxidizer because they contain both fuel and oxidizer in their structures.

* Corresponding author.
E-mail addresses: celalevci@yahoo.com, cevci@kho.edu.tr (C. Evci).

http://dx.doi.org/10.1016/j.applthermaleng.2016.04.062
1359-4311/© 2016 Elsevier Ltd. All rights reserved.

Nomenclature

a	inner radius
A	barrel cross section
α	heat expansion coefficient
b	outer radius
C	specific heat
d	barrel inside diameter
D	difference
$\frac{dr}{dt}$	burn rate
θ	circumferential coordinate
E	modulus of elasticity
ε	strain
$\varnothing$	fraction of propellant burnt
h	convection heat transfer coefficient
k	thermal conductivity
m	mass
μ_d	the mean of differences of the batch
n	propellant constant
N	number of data
Nu	Nusselt number
P	mean pressure in the barrel
Pr	Prandtl number
ρ	density
q	heat generation per unit volume
r	radial coordinate
R	gas constant
Re	Reynolds number
σ	stress
$\varnothing$	stress function
t	time
T	temperature
T_0	adiabatic flame temperature
V	combustion chamber volume
v	Poisson's ratio
w	web thickness
x	distance moved by the bullet
X	experimental data
Y	numerical data
z	axial coordinate
$Z_{\alpha/2}$	standard normal distribution value

Subscripts

E	equivalent
θ	circumferential
g	gas
i	inner
o	outer
r	radial
s	solid propellant
z	axial

Bullets in conventional weapon systems get their propulsion and spin energies while being inside the barrel and only from solid propellant fuels or gun powders. During shots, the barrel experiences high internal pressure and temperature. Because of the complexity of solid propellant combustion inside the barrel, computations are performed based on certain assumptions [2–7]. Parameters such as temperature, compressibility and gas volume of combustion products are determined using the ideal gas law [1–3] and the assumption that the solid propellant is burned in a single step under atmospheric conditions [7]. Temperature and heat transfer coefficient as a function of pressure can be calculated using the internal conditions of the barrel which are modified according to atmospheric data [7].

Under different pressures, solid propellants show different combustion behaviors and burn rates. Burn rate increases with respect to increasing internal pressure and temperature. Thus, as propellant temperature increases, pressure at the end of combustion chamber increases and combustion duration decreases. It has been determined that the addition of high energy materials into composite modified double base (CMDB) propellants increases combustion pressure and burn rate. Burn rate is a strong function of burn surface area, grain shape and internal pressure [8–13].

The heat transfer through the inner wall of the barrel and thermal stresses can be predicted using various approximations. Heat transfer occurring in large caliber weapons causes wear and failure on the barrel surface. In order to reduce the heating for successive shots, cooling of the barrel has been investigated by creating cooling channels at the joints of the two-part barrel. Thermal stresses and erosion on the inner wall of the barrel are important due to high thermal and pressure loads. Thermo-mechanical cracking and wear mechanisms for large caliber guns have been investigated in detail. Initial temperature and grain size of the solid propellant has an important effect on the ballistics performance and the barrel heating [14–18].

In this work, combustion characteristics of double base propellants (85% Nitrocellulose and 15% Nitroglycerine) with various grain sizes and initial temperatures were determined by performing a series of shooting tests and employing a thermo-mechanical model setup with ABAQUS® finite element code. Effects of various grain sizes (300–425, 425–500, 500–600, 600–710, 710–850 μm) and initial temperatures (−60, −20, 0, 20, and 60 °C) of double base propellants on internal pressure, bullet velocity and barrel heat transfer were investigated experimentally and computationally. Samples of propellants were tested in a shooting range by using a NATO standard small caliber barrel of 7.62 mm in diameter, and barrel internal pressure, bullet velocity and barrel surface temperatures were measured experimentally. The events that occur in the barrel during burning of the propellant are very complex and it is not easy to determine the ballistic parameters and the temperature/stress distribution along the barrel axis. It is not possible to measure the temperature distribution in the barrel experimentally where the temperature values are required to determine the thermal stress distribution in the barrel. So, the temperature distribution was tried to obtain numerically. FEA analysis is conducted to determine the distribution of temperature, stress and displacement under coupled thermal and mechanical loading. The developed numerical model was experimentally validated for the interior ballistics problem based on the propellant grain size at different conditioning temperatures. Outer surface temperature of the barrel was measured using thermocouples and compared to the model solution. In addition, inner wall temperature of the barrel was determined as a function of the shooting frequency using FEA. The developed model of this study can be used in other studies with the least experimental work to offer convenient solutions for various parametric studies.

2. Theoretical formulation

This study is based on an analysis of the impulsive gaseous mixture from the burning of a gun powder consisting of 85% Nitrocellulose and 15% Nitro-glycerin in a barrel. The chemical reaction is given in Eq. (1) [7].

$$17C_{24}H_{30}(NO_2)_{10}O_{20} + 3C_3H_5(NO_3)_3 \rightarrow 250CO_2 + 167CO + 40H_2O + 222.5H_2 + 89.5N_2 + 1000\,\text{cal/g} \quad (1)$$

Solid propellant fuels provide chemical energy, which is converted to kinetic energy for conventional bullets to spin and move along the weapon barrel. Thus, burn rate is one of the most important design parameters for bullet performance and range. Burn rate depends on many factors including combustion pressure, grain geometry, temperature, energetic materials, combustion sensitivity, chemical ingredients, percentage of oxidized materials and ignition energy. In solid propellants, combustion starts from the outer surface and propagates perpendicular to the burning surface, expanding radially outward or inward depending on the geometry of the propellant [1–6]. Although the burning event of the solid rocket propellants is quite complex, its mathematical model is sufficiently established and the rate of change of the solid propellant as the burn rate can be expressed as [1–7]:

$$w\frac{dr}{dt} = -kTP^n \quad (2)$$

where dr/dt is the burn rate (mm/s), T is the temperature (°K), w is the minimum distance between the burning surfaces (web thickness), P (kPa) is the pressure, and k and n are the experimental constants. Thermo-mechanical characteristics of propellants affect the value of n. For fast burn, $0 \leqslant n \leqslant 1$ and for slow burn, $0.3 \leqslant n \leqslant 0.8$. The value of k is a function of grain shape, temperature and calorific value. It is equal to 1 before combustion starts and 0 after combustion ends. The value of dr/dt is equivalent to the combustion rate and it indicates how fast propellant is consumed. As the solid propellant burns in a contained chamber, some of the solid phase is transformed to the gas phase as follows:

$$m_g(t) \cong \varnothing(t)m_s \quad (3)$$

where t is the time, m_g is the mass of the solid transformed to the gas phase, m_s is the mass of solid propellant, $\varnothing$ is the fraction of propellant burnt within $0 \leqslant \varnothing \leqslant 1$. In Fig. 1, the schematic showing the relation between the solid and gas phases is given. The fraction of propellant burnt can be expressed as

$$\varnothing = (1 - r)(1 + \theta r) \quad (4)$$

where θ changes based on the shape factor and is an indication of the change of the burnt surface. As θ increases, the surface decreases faster and the rate of evolution of gases at constant pressure drops faster. Shapes of positive θ are designated as "degressive", negative θ to be "progressive" and those with $\theta = 0$ are called "neutral".

If Eqs. (2) and (4) are combined, the fraction of propellant burnt can be expressed in terms of shape factor and pressure as

$$w\frac{d\varnothing}{dt} = kP(t)[(1+\theta)^2 - 4\theta\varnothing(t,T)]^{1/2} \quad (5)$$

Propellant grains, based on their combustion surfaces, can be classified as regressive, neutral and progressive burning. If there is a central core, it is usually a neutral burning grain. If the grain is cylindrical, spherical and cubical, it is regressive burning. And, multi-perforated grains are usually progressive burning [10]. Fig. 2 shows the fraction of propellant burnt as a function of the burning rate for different shapes. This figure implies that fraction of propellant burnt is a function of propellant burning rate which depends on the shape (form) factor related to the geometry of propellant. For any shape of the propellant grain, there is a strict relationship between the fraction of propellant burnt and the fraction of grain size (ballistic size) which is unburnt. This relationship called as the form function determines whether the nature of burning is progressive or degressive. θ in Fig. 2 is the shape factor (also defined by Eq. (4)) which is a measure of the change in the area of the burning surface as burning proceeds (constant for a given shape) [2]. A larger value of θ means that burning surface decreases faster as a result of increasing area of the burning surface. This situation alters the distribution of barrel internal pressure and maximum pressure point in the barrel.

For the modeling of propellant burn in barrels, there are several stages as (a) propellant burning at constant volume, (b) movement of the bullet, (c) gases reaching the maximum pressure (d) fully consumed propellant [2,5]. Fig. 3 shows these various stages. Propellant burn related to these stages can be summarized as follows:

(1) During combustion, before the bullet starts moving, the propellant starts burning after the ignition and gases with high temperature are produced. It is assumed that all grain particles start burning at the same time [2,6]. The bullet starts moving once the internal pressure overcomes all the friction forces inside the barrel. These events occur at constant volume. The corresponding gas equation can be written as

$$P(t)\left(V - m_s\left(\frac{1-\varnothing(t)}{\rho}\right)\right) = \varnothing(t)m_sRT_0 \quad (6)$$

where P is the pressure, V is the volume of the combustion chamber, m_s is the mass of the propellant, ρ is the density of the propellant, R is the ideal gas constant, and T_0 is the adiabatic flame temperature.

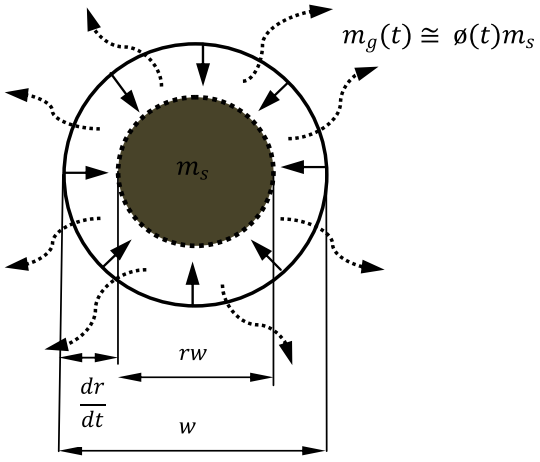


Fig. 1. Schematic of a solid propellant of spherical geometry transforming to the gas phase.

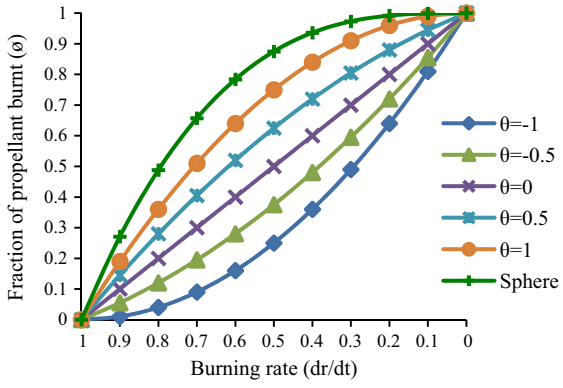


Fig. 2. The fraction of propellant burnt as a function of the burning rate and shape factor.

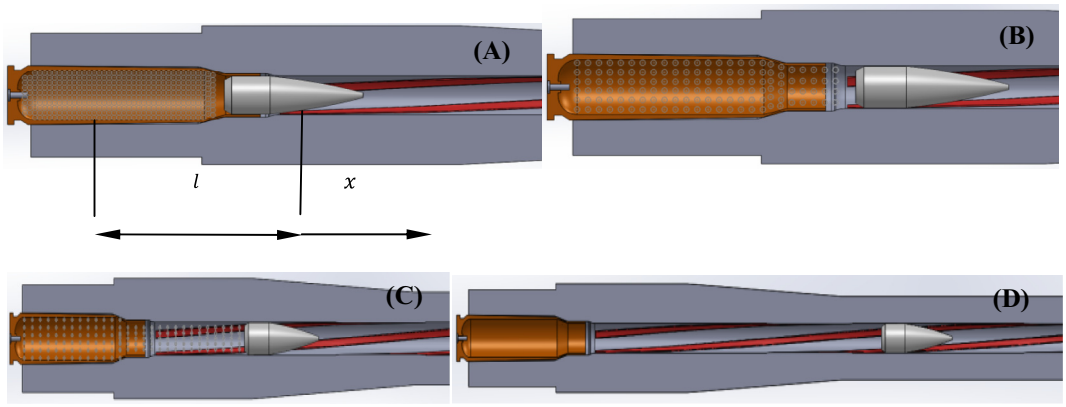


Fig. 3. Four stages of propellant burn in barrel: (A) Propellant burn at constant volume, (B) movement of the bullet, (C) reaching maximum pressure, and (D) fully consumed propellant.

(2) The propellant burns out after the maximum pressure is achieved [6]. Because the bullet moves during this stage, the combustion occurs while volume changes. During this stage, the following relation can be written [2]

$$P(t)\left(V + Ax - m_s\left(\frac{1-\varnothing(t)}{\rho}\right)\right) = \varnothing(t) m_s R T_0 \tag{7}$$

where A is the cross section of the barrel, and x is the distance the bullet has traveled.

(3) After the propellant is consumed, only the gas phase exists in the system and high pressure/temperature expands the gases which push the bullet forward. The following equation can be written for this stage

$$P(t)(V + Ax) = m_g R T_0 \tag{8}$$

As the temperature in the barrel changes, the density of the gases will change as well, and can be calculated using the ideal gas law [1–3]

$$\rho = \frac{P}{R T_g} \tag{9}$$

where T_g is the gas temperature already introduced in Eq. (6) as T_0.

The Nusselt number is calculated from [19]

$$Nu = 0.023 Re^{0.8} Pr^{0.3} \tag{10}$$

$$Re = \frac{\rho V_g d}{\mu} \tag{11}$$

where Re is the Reynolds number, Pr is the Prandtl number, d is the barrel inside diameter, V_g is the velocity of gases along the barrel and μ is the dynamic viscosity. Subsequently, the convection heat transfer coefficient of the gas (h_g) is calculated from

$$h_g = \frac{k Nu}{d} \tag{12}$$

All the values of μ, R, Pr, k in above equations are calculated according to the gas mixture law.

The general form of three-dimensional transient heat conduction equation in cylindrical coordinates is

$$\frac{1}{r}\frac{\partial}{\partial r}\left(kr\frac{\partial T}{\partial r}\right) + \frac{1}{r^2}\frac{\partial}{\partial \theta}\left(k\frac{\partial T}{\partial \theta}\right) + \frac{\partial}{\partial z}\left(k\frac{\partial T}{\partial z}\right) + \dddot{q} = \rho C \frac{\partial T}{\partial t} \tag{13}$$

where r, θ, z are the radial, circumferential and axial coordinates, k thermal conductivity (W/m^2 K), $\dddot{q}$ the heat generation per unit volume (W/m^3), ρ the density, C the specific heat (J/kg K), t the time, and T the temperature.

The initial and boundary conditions of heat transfer problem in the barrel (with inner and outer radii of a and b) are given as

$$T(r,t) = T_\infty \quad \text{for } t = 0, \quad a \leqslant r \leqslant b \tag{14}$$

for $t > 0$,

$$h_g(T_g - T_i) = -k\left.\frac{\partial T}{\partial r}\right|_{r=a}$$

$$h_{air}(T_o - T_\infty) + \varepsilon\sigma(T_o^4 - T_{surr}^4) = -k\left.\frac{\partial T}{\partial r}\right|_{r=b} \tag{15}$$

where h_g and h_{air} are the convection heat transfer coefficients corresponding to the gas generated in the barrel and outside air, T_i, T_o are the inner and outer surface temperatures of the barrel, T_g is the gas temperature in the barrel, T_∞ is the temperature of the air nearby the outer surface of the barrel, T_{surr} is the absolute temperature of the surrounding surface enclosing the barrel surface for the radiation heat transfer, a and b are the inner and outer radii of the barrel, ε is the emissivity of the barrel surface, σ is the Stefan–Boltzmann constant.

The temperature distribution in the gun barrel is assumed to be circumferentially axisymmetric so that temperature varies only in the radial direction through the wall thickness at any position of the projectile along the barrel. At a specified position of the bullet in the barrel, steady state temperature distribution assumed and axial dependence of the temperature is ignored as well. With these assumptions Eq. (13) reduces to

$$\frac{1}{r}\frac{\partial}{\partial r}\left(kr\frac{\partial T}{\partial r}\right) + \dddot{q} = 0 \tag{16}$$

Solving Eq. (14), the temperature distribution in the radial direction is obtained as

$$T(r) = -\frac{\dddot{q}}{4k} r^2 + C_1 \ln r + C_2 \tag{17}$$

The integration constants C_1 and C_2 in Eq. (17) are obtained using the boundary conditions of temperature in the inner and outer surfaces of the cylinder.

$$\begin{aligned} r = a \;&\rightarrow\; T(a) = T_i = -\frac{\dddot{q}}{4k} a^2 + C_1 \ln a + C_2 \\ r = b \;&\rightarrow\; T(b) = T_o = -\frac{\dddot{q}}{4k} b^2 + C_1 \ln b + C_2 \end{aligned} \tag{18}$$

where a is the inner radius, T_i the inner wall temperature, b the outer radius, T_o the outer wall temperature. Solving for the

constants C_1 and C_2, the temperature distribution in radial direction is obtained as

$$T(r) = T_i + \frac{\dddot{q}}{4k}(a^2 - r^2) + \left[\frac{\dddot{q}}{4k\ln(\frac{a}{b})}(a^2 - b^2) + \frac{T_i - T_0}{\ln(\frac{a}{b})}\right]\ln\frac{r}{a} \quad (19)$$

Since the combustion and heat transfer process occurs within milliseconds, heat transfer in the barrel may be assumed to occur adiabatically which implies that $\dddot{q} = 0$. Finally, the radial temperature distribution through the barrel wall thickness takes the following form

$$T(r) = T_i + \left(\frac{T_i - T_0}{\ln(\frac{a}{b})}\right)\ln\frac{r}{a} \quad (20)$$

The barrel is considered as a thick walled cylinder with open end that is axially free to expand [20]. The barrel is subjected to both mechanical and thermal stresses generated due to high pressure and temperatures emanating from propellant burning. Generalized Hooke's law is applied to thick walled cylinder of the gun barrel in the elastic range to obtain the radial, circumferential and axial strains as

$$\varepsilon_r = \frac{1}{E}(\sigma_r - \nu(\sigma_\theta + \sigma_z)) + \alpha T \quad (21)$$

$$\varepsilon_\theta = \frac{1}{E}(\sigma_\theta - \nu(\sigma_r + \sigma_z)) + \alpha T \quad (22)$$

$$\varepsilon_z = \frac{1}{E}(\sigma_z - \nu(\sigma_r + \sigma_\theta)) + \alpha T \quad (23)$$

where ε_r, ε_θ, ε_z are the radial, circumferential and axial strains, σ_r, σ_θ, σ_z are the radial, circumferential and axial stresses, E is the elastic modulus, ν is the Poisson's ratio and α is the thermal expansion coefficient.

Axisymmetric loading condition as a result of the internal pressure may be assumed which imply that all points on an annular element of the barrel wall displace by the same amount just depending on the radius. Moreover, the radial shape of the barrel is maintained which implies that there can be no shears on radial and tangential planes. The barrel is axially free to expand and it is assumed that axial strain is constant ($\varepsilon_z = \varepsilon_0$), i.e. plane sections remain plane. Using Eq. (23), the axial stress is obtained as

$$\sigma_z = \nu(\sigma_r + \sigma_\theta) + E(\varepsilon_0 - \alpha T) \quad (24)$$

Eq. (24) is substituted into Eqs. (21) and (22) to express the radial and circumferential strains in the following form

$$\varepsilon_r = \frac{1}{E}\left[(1 - \nu^2)\sigma_r - \nu(1 + \nu)\sigma_\theta - \nu\varepsilon_0 E + (1 + \nu)E\alpha T\right] \quad (25)$$

$$\varepsilon_\theta = \frac{1}{E}\left[(1 - \nu^2)\sigma_\theta - \nu(1 + \nu)\sigma_r - \nu\varepsilon_0 E + (1 + \nu)E\alpha T\right] \quad (26)$$

The stress-equilibrium relation is given by

$$\frac{d\sigma_r}{dr} + \frac{\sigma_r - \sigma_\theta}{r} = 0 \quad (27)$$

The equilibrium equation (Eq. (27)) is satisfied if the stress function $\varnothing$ is introduced such that [21,22]

$$\sigma_r = \frac{\varnothing}{r} \quad (28)$$

$$\sigma_\theta = \frac{d\varnothing}{dr} \quad (29)$$

The general strain–displacement relations ($\varepsilon_r = \frac{du}{dr}$, $\varepsilon_\theta = \frac{u}{r}$ where u and r are the radial displacement and the radial coordinate, respectively) can be combined as a compatibility equation:

$$\frac{\varepsilon_r - \varepsilon_\theta}{r} - \frac{d\varepsilon_\theta}{dr} = 0 \quad (30)$$

The stress functions given by Eqs. (28) and (29) are substituted in Eqs. (25) and (26) which are implemented into the compatibility equation given by Eq. (30), and then the resulting equation is

$$\frac{1}{rE}\left[(1 - \nu^2)\frac{\varnothing}{r} - \nu(1 + \nu)\frac{d\varnothing}{dr} - (1 - \nu^2)\frac{d\varnothing}{dr} + \nu(1 + \nu)\frac{\varnothing}{r} - r(1 - \nu^2)\frac{d^2\varnothing}{dr^2} + \nu(1 + \nu)r\left(\frac{1}{r}\frac{d\varnothing}{dr} - \frac{\varnothing}{r^2}\right) - (1 + \nu)E\alpha r\frac{dT}{dr}\right] = 0 \quad (31)$$

Rearranging Eq. (31), the final form of the compatibility equation can be obtained as

$$\frac{d^2\varnothing}{dr^2} + \frac{1}{r}\frac{d\varnothing}{dr} - \frac{1}{r^2}\varnothing = -\frac{E\alpha}{1 - \nu}\frac{dT}{dr} \quad (32)$$

Solution of the differential Eq. (32) yields

$$\varnothing = C_1 r + \frac{C_2}{r} - \frac{E\alpha}{r(1 - \nu)}\int Trdr \quad (33)$$

Substituting Eq. (20) in Eq. (33) and getting the integral, the stress function $\varnothing$ takes the form

$$\varnothing = C_1 r + \frac{C_2}{r} - \frac{E\alpha}{2(1 - \nu)}r\left[T_i + \left(\frac{T_i - T_0}{\ln\frac{a}{b}}\left(\ln\frac{r}{a} - \frac{1}{2}\right)\right)\right] \quad (34)$$

Substituting Eq. (34) in Eq. (28), the radial stress component can be obtained as

$$\sigma_r = \frac{\varnothing}{r} = C_1 + \frac{C_2}{r^2} - \frac{E\alpha}{2(1 - \nu)}\left[T_i + \left(\frac{T_i - T_0}{\ln\frac{a}{b}}\left(\ln\frac{r}{a} - \frac{1}{2}\right)\right)\right] \quad (35)$$

Applying the boundary conditions to the radial stresses, following equations are obtained:

$$\sigma_r(r = a) = -P_i = C_1 + \frac{C_2}{a^2} - \frac{E\alpha}{2(1 - \nu)}\left[T_i - \frac{1}{2}\left(\frac{T_i - T_0}{\ln\frac{a}{b}}\right)\right] \quad (36)$$

$$\sigma_r(r = b) = -P_o = C_1 + \frac{C_2}{b^2} - \frac{E\alpha}{2(1 - \nu)}\left[T_i + \left(\frac{T_i - T_0}{\ln\frac{a}{b}}\left(\ln\frac{b}{a} - \frac{1}{2}\right)\right)\right] \quad (37)$$

where P_i and P_o are the internal and external pressures.

Eqs. (36) and (37) are solved simultaneously to determine the constants C_1 and C_2. For the gun barrel the outer pressure is, $P_o = 0$. Defining $n = a/b$ and $\Delta T = T_i - T_o$, the radial and circumferential stress components are obtained as

$$\sigma_r = \frac{P_i}{n^2 - 1} + \frac{E\alpha}{2(1 - \nu)}\frac{n^2 T_0 - T_i}{n^2 - 1} + \frac{E\alpha}{4(1 - \nu)}\frac{\Delta T}{\ln n} + \frac{b^2}{(n^2 - 1)r^2}\left[-P_i + \frac{E\alpha\Delta T}{2(1 - \nu)}\right] - \frac{E\alpha}{2(1 - \nu)}\left[T_i - \frac{\Delta T}{\ln n}\left(\ln\frac{r}{a} - \frac{1}{2}\right)\right] \quad (38)$$

$$\sigma_\theta = \frac{P_i}{n^2 - 1} + \frac{E\alpha}{2(1 - \nu)}\frac{n^2 T_0 - T_i}{n^2 - 1} + \frac{E\alpha}{4(1 - \nu)}\frac{\Delta T}{\ln n} - \frac{b^2}{(n^2 - 1)r^2}\left[-P_i + \frac{E\alpha\Delta T}{2(1 - \nu)}\right] - \frac{E\alpha}{2(1 - \nu)}\left[T_i + \frac{1}{2}\frac{\Delta T}{\ln n}\right] + \frac{1}{2(1 - \nu)}\frac{E\alpha\Delta T}{\ln n}\left(1 + \ln\frac{r}{a}\right) \quad (39)$$

At the free end of the gun barrel the resulting forces should be zero which implies that

$$\int_a^b \int_0^{2\pi} \sigma_z d\theta r dr = 0 \quad (40)$$

where $\sigma_z = \nu(\sigma_r + \sigma_\theta) + E(\varepsilon_0 - \alpha T)$. Rearranging Eq. (40), the following form of equality can be obtained

$$\int_a^b \left[\frac{2\nu P_i}{n^2-1} + \frac{\nu E\alpha}{(1-\nu)}\frac{n^2T_0 - T_i}{n^2-1} + \frac{\nu E\alpha}{2(1-\nu)}\frac{\Delta T}{\ln n} - \frac{\nu E\alpha T_i}{(1-\nu)} + \frac{\nu E\alpha\Delta T}{(1-\nu)\ln n}\ln\frac{r}{a} + E(\varepsilon_0 - \alpha T)\right] r dr = 0 \tag{41}$$

Eq. (41) is solved to get the constant axial strain ε_0 as

$$\varepsilon_0 = \alpha T_i + \frac{\alpha\Delta T}{2(1-\nu)\ln n} - \frac{\alpha\Delta T a^2}{(1-\nu)(b^2-a^2)} - \left[\frac{2\nu P_i}{E(n^2-1)} + \frac{\nu\alpha}{(1-\nu)}\frac{n^2T_0 - T_i}{n^2-1} + \frac{\nu\alpha}{2(1-\nu)}\frac{\Delta T}{\ln n} - \frac{\nu\alpha T_i}{(1-\nu)}\right] \tag{42}$$

Substituting Eq. (42) in Eq. (24), the axial stress component is obtained as

$$\sigma_z = \nu\left[\frac{2P_i}{n^2-1} + \frac{E\alpha}{(1-\nu)}\frac{n^2T_0 - T_i}{n^2-1} + \frac{E\alpha}{2(1-\nu)}\frac{\Delta T}{\ln n} - \frac{E\alpha T_i}{(1-\nu)} + \frac{E\alpha\Delta T}{(1-\nu)\ln n}\ln\frac{r}{a}\right] + E\left[\alpha T_i + \frac{\alpha\Delta T}{2(1-\nu)\ln n} - \frac{\alpha\Delta T a^2}{(1-\nu)(b^2-a^2)} - \left(\frac{2\nu P_i}{E(n^2-1)} + \frac{\nu\alpha}{(1-\nu)}\frac{n^2T_0 - T_i}{n^2-1} + \frac{\nu\alpha}{2(1-\nu)}\frac{\Delta T}{\ln n} - \frac{\nu\alpha T_i}{(1-\nu)}\right) - \alpha\left(T_i - \left(\frac{T_i - T_0}{\ln n}\right)\ln\frac{r}{a}\right)\right] \tag{43}$$

The Von Mises stresses corresponding to the stress state of principal stresses which are radial, circumferential and axial stresses (given by Eqs. (38), (39) and (43), respectively) in the barrel are obtained by

$$2\sigma_E^2 = (\sigma_\theta - \sigma_r)^2 + (\sigma_r - \sigma_z)^2 + (\sigma_z - \sigma_\theta)^2 \tag{44}$$

3. Experimental study

The shooting tests were conducted with double based 7.62 × 51 mm standard NATO ammunition. Ballistic tests were performed with a special test barrel. In the tests, magazines with a capacity of 10 cartridges were used. Bullets were 9.5 g and the solid propellant was 2.8 g. Double base propellants with various grain sizes (300–425, 425–500, 500–600, 600–710, 710–850 μm) and initial temperatures (−60, −20, 0, 20, and 60 °C) were employed in a series of shooting tests to determine the internal pressure, bullet velocity and barrel outer surface temperature, experimentally.

Ballistic tests were performed according to AEP-97 [23]. The maximum pressure in the barrel was measured by using piezoelectric transducer (brand: Kishler) located at the maximum pressure point which is 50 mm far away from the starting point of lands and grooves. The bullet velocity was calculated using the arrival times of the strain pulse jumps corresponding to the bullet position where strain gages were installed. Kyowa brand strain gages with resistance of 350 ohms and J type Elimko brand thermocouples were mounted on the barrel outer surface. The first strain gage and thermocouple were located at the point where barrel lands and grooves started and following strain gages and thermocouples were located at 25 mm with respect to each other. Dewesoft Sirius data acquisition system having 40 channels with data rates 200 kHz was used to get the test data. Fig. 4 presents the test equipment, data acquisition system, and installation of thermocouples and strain gages at 24 points of the barrel. Barrel internal pressure and bullet velocity as functions of displacement and time were measured experimentally using 24 strain gages on the outer surface and 2 piezoelectric sensors on the inner surface. Fig. 5 shows the pressure distribution inside the barrel as a function of displacement along the barrel axis. Fig. 5A presents the pressure distribution for various grain sizes of the propellant while Fig. 5B gives the pressure distribution of the propellant with 500–600 μm grain size at different initial temperatures. The outer surface temperatures of the barrel were measured using J thermocouples and data was gathered for every 0.5 s. Repeated tests with each grain size of the propellant and different initial temperatures were performed to get more accurate and consistent results. Also, the muzzle velocity was measured using a Doppler radar.

4. Thermo-mechanical modeling

Combustion gases due to complex thermo-chemical reactions inside the barrel provide propulsion and spin energies to bullets. During these reactions, dynamic internal temperatures and

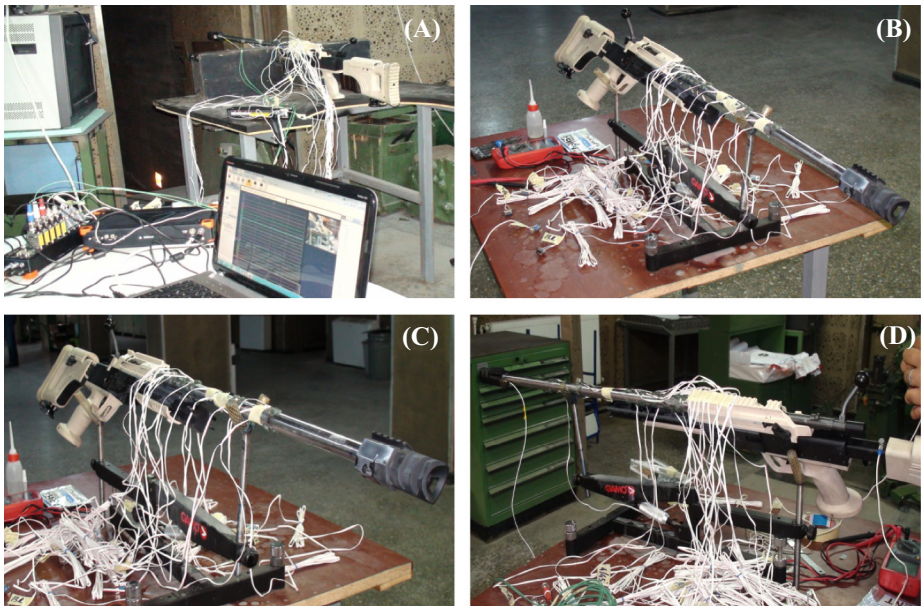


Fig. 4. Test equipment with (A) data acquisition system, (B) barrel with 24 sections, (C) thermocouple installation, and (D) strain gage installation.

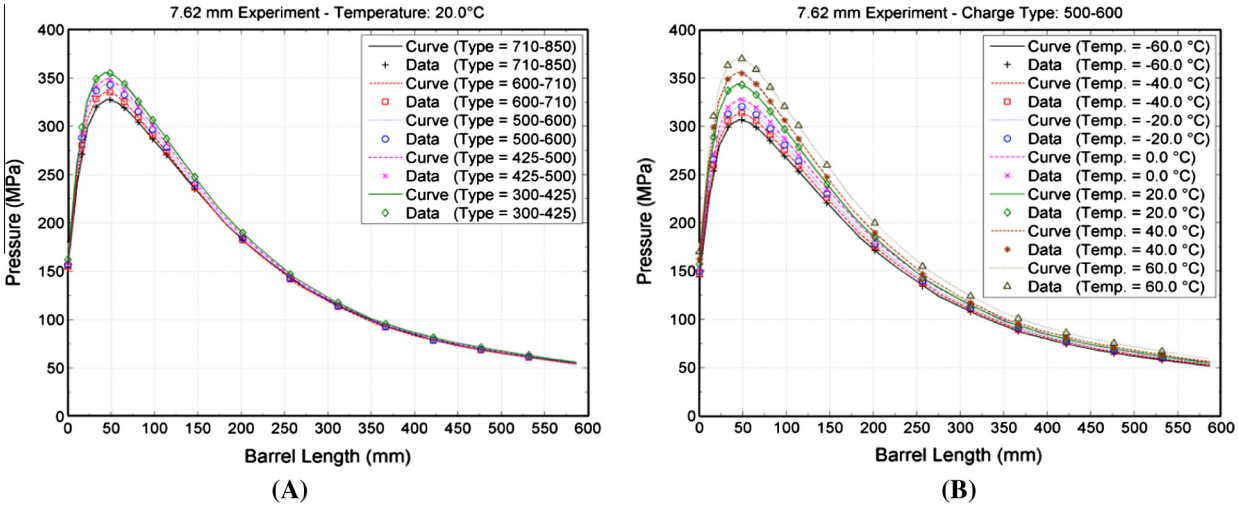


Fig. 5. Pressure inside the barrel as a function of displacement: (A) for various grain sizes and (B) at different initial temperatures of the propellant.

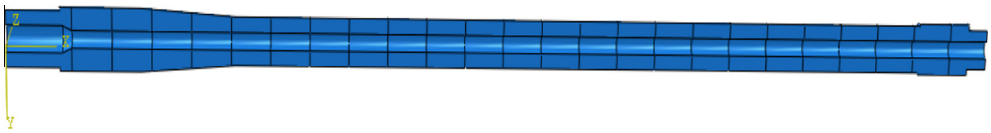


Fig. 6. FEA model of the barrel in ABAQUS.

pressures occur. The period of successive shots can be expressed in two stages as shooting and preparation. During the shooting period, the solid propellant starts burning, the bullet moves and reaches the tip of the barrel and these events take 1.34 ms. Preparation period includes the waiting time between two successive shots.

Half of the actual barrel was modeled in ABAQUS with 660 mm of length, 7.7 mm of inner diameter and without helical grooves as seen in Fig. 6. In order to apply the loads to the area of the helical grooves, the barrel was divided into 24 pieces with 25 mm of length and materials properties were expressed according to Fig. 7. The period of successive shots is defined as the combination of shooting period and preparation period. The preparation time was set at different periods of 1, 3, 5 and 10 s. The barrel was fixed at the point of contact with the weapon. Also, in order to reduce the computational overhead, a half-symmetry was used.

During experiments, 10 successive shots were achieved and resulting temperature and pressure data were measured. The computational model was built based on these periods and experimental conditions as much as possible. In the model, internal pressure data were entered as functions of displacements and time. For successive shots, loading effects such as left-over pressure and temperature from the previous shot was added to the loading of the current shot. Calculated pressure loadings were applied to each of 24 sections of the barrel.

Table 1
Outer surface temperatures at the maximum pressure point in the barrel for different meshes.

			Outer surface temperature (°C)
Experimental			117.4
	Number of meshes	Number of nodes	
Numerical	11,218	15,086	120.8
	21,574	29,010	129.2
	44,442	59,760	129.5

To check for the mesh independency the barrel was analyzed with different mesh sizes and nodes. The outer surface temperatures of the barrel for different mesh sizes and corresponding

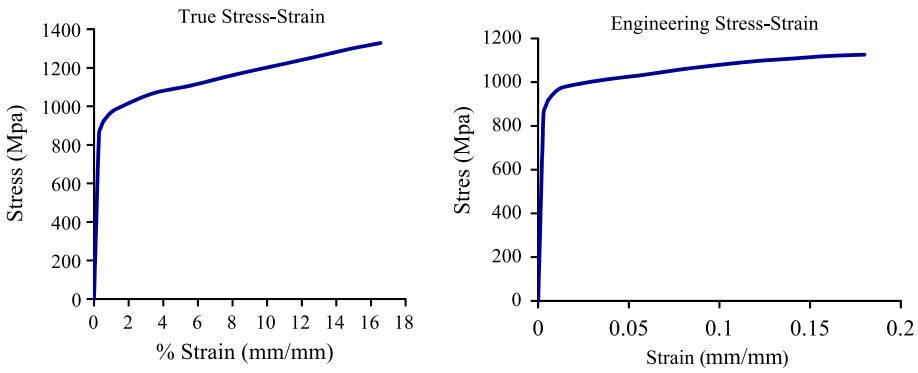


Fig. 7. Stress–strain relations of the barrel material.

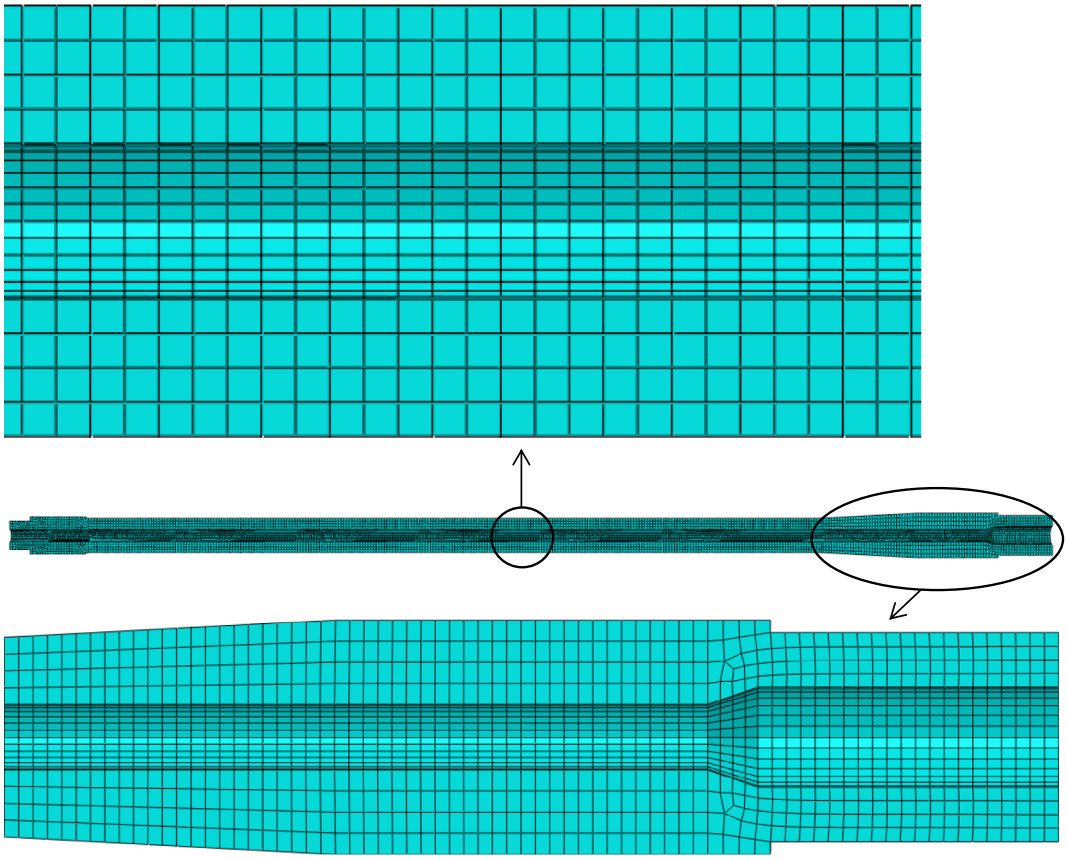


Fig. 8. Mesh of the barrel in ABAQUS.

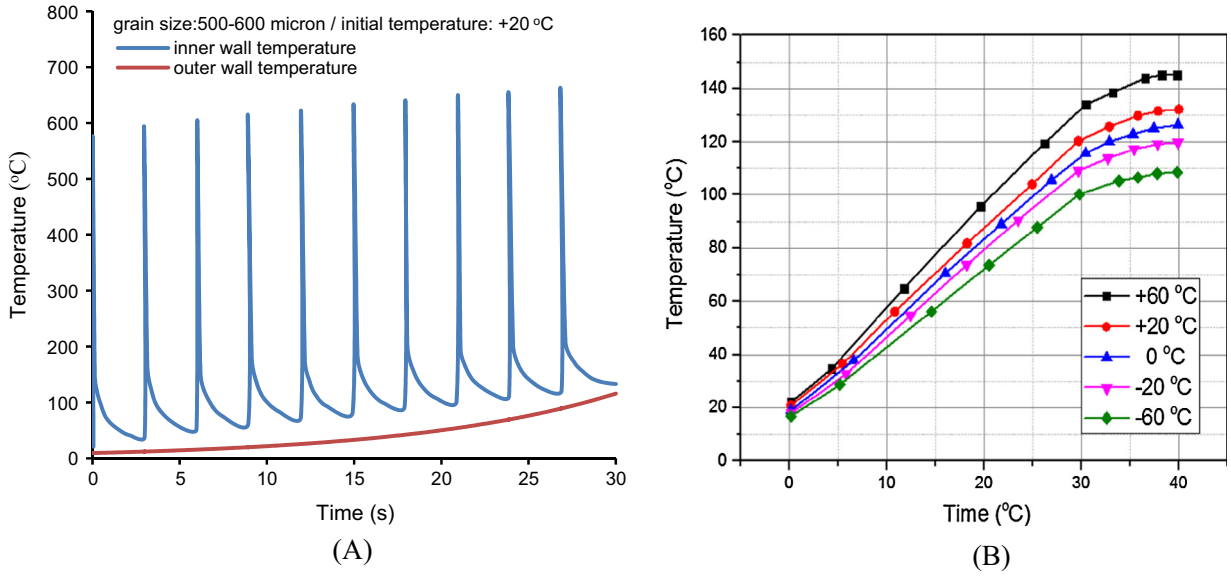


Fig. 9. Temperatures of (A) the inner and outer walls as a function of time for the solid propellant with 500–600 μm grain size at an initial temperature of 20 °C and (B) the outer wall for different initial temperatures of the propellant.

nodes are given in Table 1. FEA of the barrel model in ABAQUS employed a total number of 21,574 mesh elements and 29,010 nodes (see Fig. 8) as a result of acceptable accuracy with a reasonable computation time.

Interior ballistics parameters such as gas temperature, the convection heat transfer coefficient and inner wall temperature were calculated using the relevant equations derived in Section 2, "theoretical formulation" and applied to the FEA model. Thermo-mechanical element type was used in the FEA analysis. Nodes were created at the highest pressure points on the inner and outer surfaces of the barrel. Analyses were performed at the periods of 1, 3, 5 and 10 s. As the time increased between successive shots, temper-

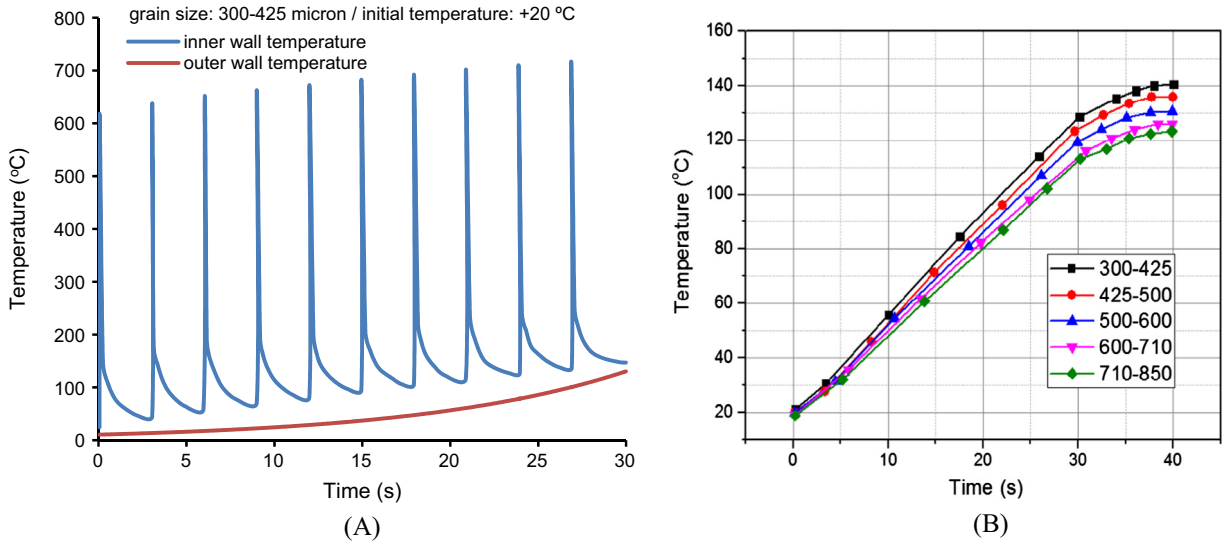


Fig. 10. Temperatures of (A) the inner and outer walls as a function of time for the solid propellant with 300–425 μm grain size at an initial temperature of 20 °C and (B) the outer wall temperatures for different grain sizes of the propellant at 20 °C.

atures of the inner and outer surfaces got closer to each other. As shots for different periods are analyzed, the outer surface temperature of the barrel increased less with the increase of the shooting period.

During the shooting the inner wall temperature increased suddenly and as soon as the bullet left the barrel the temperature decreased. The outer wall temperature increased with a certain behavior (see Fig. 9A). After the shooting, the inner wall temperature decreased while the outer wall temperature increased. Finally, equilibrium was achieved and both wall temperatures decreased. Temperatures of the inner and outer walls as a function of time for the solid propellant with 500–600 μm grain size at an initial temperature of 20 °C is given in Fig. 9A. Fig. 9B displays the outer wall temperatures of the barrel in which solid propellants with 500–600 μm grain size at different initial temperatures (varying from −60 °C to +60 °C) were employed. On the other hand, Fig. 10 displays the temperatures of the inner and outer walls as a function of time for the solid propellant with various grain sizes (300–425, 425–500, 500–600, 600–710, and 710–850 μm) at an initial temperature of 20 °C. Figs. 9 and 10 clearly reveal that the barrel heats up with respect to higher initial temperature and smaller grain size which makes the burn rate increase.

5. Validation of numerical model using paired *t*-test

Paired *t*-test analysis based on the comparison of two different methods of measurements is employed to two sets of temperature measurements from the outer surface of the barrel. Using this analysis a confidence interval for the difference between the two temperature means based on the paired differences of numerical and experimental data is determined. The difference between the experimental and numerical temperature values is defined by

$$D_j = X_j - Y_j \quad j = 1, 2, \ldots, N \tag{45}$$

where N is the total number of data to be analyzed, D is the difference, X_j is the experimental data and Y_j is the numerical data. In the analysis a total of 31 temperature data were used for each pair of a particular shooting tests. Then, the mean difference is

$$\overline{D}_j = \frac{\sum_{j=1}^{N} D_j}{N} \tag{46}$$

The variance of difference is given by

Table 2
Confidence interval of numerical and experimental temperature data for particular grain sizes and conditioning temperatures.

	95% confidence interval	Comment
Tests at −60 °C	$-2.82 \leqslant \mu_d \leqslant 7.25$	No difference
Tests at +60 °C	$-13.33 \leqslant \mu_d \leqslant 11.13$	No difference
Grain size: 300–425 μm	$-4.76 \leqslant \mu_d \leqslant 6.22$	No difference
Grain size: 710–850 μm	$-3.91 \leqslant \mu_d \leqslant 1.63$	No difference

$$\mathrm{Var}(\overline{D}) = \frac{\sum_{j=1}^{N} (D_j - \overline{D})^2}{N(N-1)} \tag{47}$$

A typical confidence level of 95% is used to determine the confidence interval for the difference between the two means based on the paired temperature differences. This interval is defined as follows [24]:

$$\overline{D} - Z_{\propto/2}\sqrt{\mathrm{Var}[D(N)]} \leqslant \mu_D \leqslant \overline{D} + Z_{\propto/2}\sqrt{\mathrm{Var}[D(N)]} \tag{48}$$

where $Z_{\propto/2}$ is the standard normal distribution value and μ_D is the mean of differences of the batch.

Results of paired *t*-test analysis are presented in Table 2 for the temperature data corresponding to tests at −60 °C (the minimum test temperature) and at 60 °C (the maximum test temperature) using a propellant grain size of 500–600 μm, and at 20 °C using propellant grain sizes of 300–425 μm and 710–850 μm. Paired *t*-test analysis does not produce any meaningful difference between the two data sets which implies a real idea of the model accuracy.

6. Results and discussion

The inner and outer wall temperatures of the barrel were analyzed three-dimensionally using the ABAQUS solver. The gas temperature distribution along the barrel, which was determined using the equations from Eq. (6) to Eq. (8), and the convection heat transfer coefficient calculated from Eq. (12) constituted the input data for coupled analysis in ABAQUS. Experimental measurements from temperature readings at the locations where thermocouples were installed on the outer wall of the barrel were compared to computational results of the thermo-mechanical model for the nodes corresponding to the experimental data collection points.

The first comparison of experimental and computational study was made on the basis of maximum temperature data during 10 successive shots (with a preparation period of 3 s) with solid propellants conditioned at a range of the initial temperatures from −60 to 60 °C. Fig. 11 displays the comparison of experimental and computational temperature measurements of the barrel outer surface corresponding to the shooting tests employing solid propellant with grain size of 500–600 μm at five different initial temperatures from −60 °C to 60 °C. As seen in Fig. 11, maximum temperatures for the experimental–computational studies for different propellant initial temperatures of −60, −20, 0, 20, and 60 °C were 99.7–110.0 °C, 109.6–120.6 °C, 114.1–125.9 °C, 117.4–132.5 °C, and 136.4–145.5 °C. Increasing the initial temperature of the propellant resulted in higher barrel wall temperatures.

Temperature results of FEA solution were approximately 11% higher than that of experimental readings obtained using thermocouples. Differences between experimental and computational results are due to many factors. As an example, J-type thermocouples have slow responses and as the response time increases, heat loss (cooling) from the surface increases. This causes lower temperature measurements experimentally. Also, computational assumptions and experimental errors could affect the results. In numerical solution, propellant burning was assumed to obey Eq. (1) and complete burning of the propellant was assumed. In fact, a small quantity of the propellant remains unburnt. As a result of this, the energy released based on the numerical calculations was higher than the real situation. Consequently, numerical temperature values were higher than the experimental readings. Also, error in calculating the convection heat transfer coefficient may be another source of computational error. Although the propellant geometry used in the study was assumed to be spherical, it's not exactly spherical. Propellants, although manufactured in the same

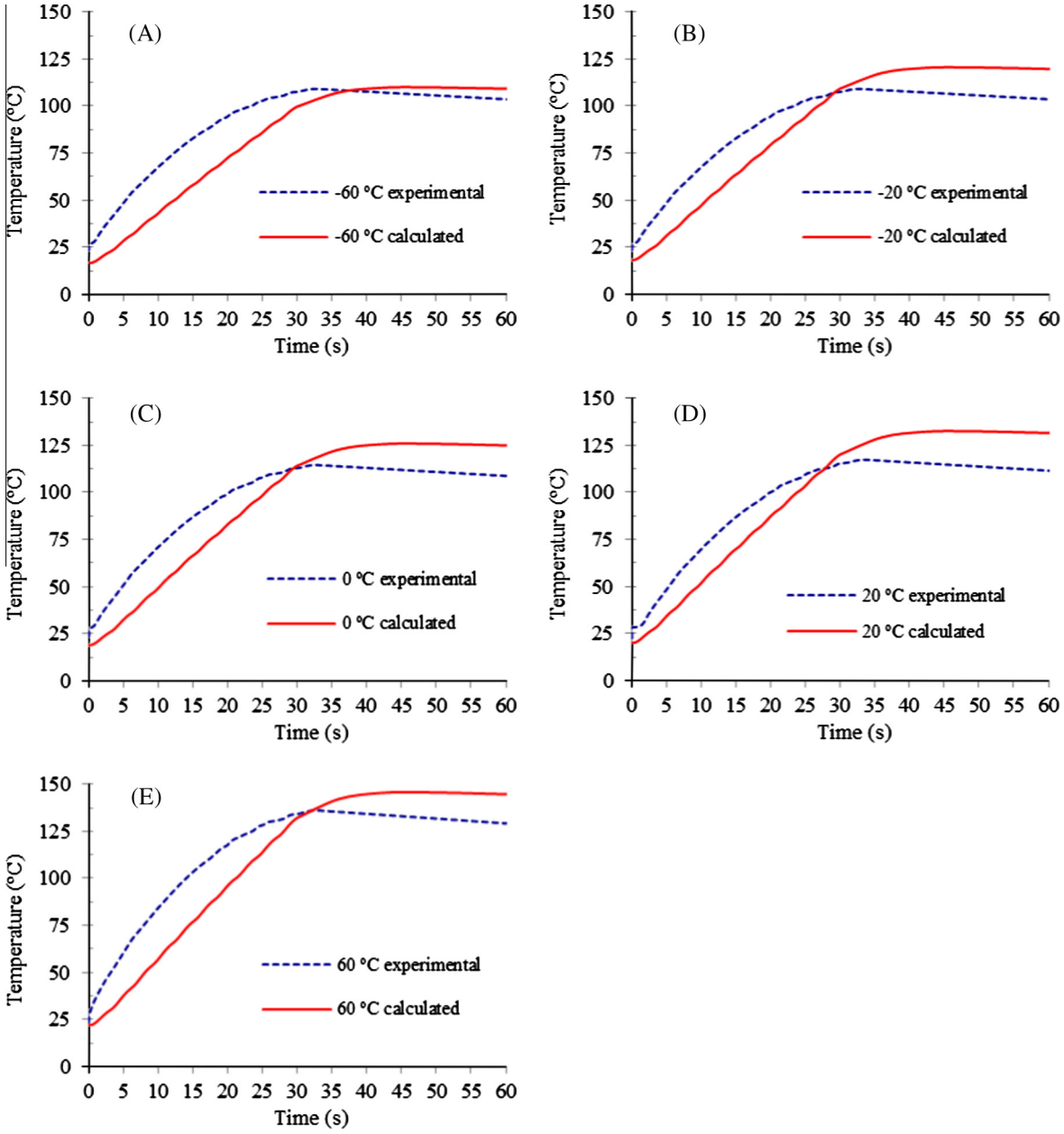


Fig. 11. Time dependent maximum temperature in the barrel corresponding to experimental–computational analysis of shooting tests at propellant initial temperatures of (A) −60 °C, (B) −20 °C, (C) 0 °C, (D) 20 °C, and (E) 60 °C.

conditions specified with a particular lot number, show slightly different characteristics. Therefore, even with the same weight of propellants of different lots the pressure values obtained were not the same. Thickness of the graphite coating on the propellant is not exactly uniform which affects the burning characteristics.

The second comparison of experimental and computational study was made for propellants of various grain sizes (300–425, 425–500, 500–600, 600–710 and 710–850 μm). Fig. 12 presents the comparison of experimental and computational temperature measurements of the barrel outer surface corresponding to the shooting tests employing solid propellants with various grain sizes of 300–425, 425–500, 500–600, 600–710 and 710–850 μm at an initial temperature of 20 °C. As seen in Fig. 12, the maximum temperatures for experimental–computational studies for grain sizes of 300–425, 425–500, 500–600, 600–710 and 710–850 μm were 126.2–141 °C, 121.4–137.8 °C, 117.4–129.2 °C, 117.1–127.2 °C and 116.6–124.6 °C, respectively. The largest deviation occurred for the tests corresponding to the grain size of 300–425 μm. The reason is that larger uncertainties occur while collecting data with a higher burn rate.

The temperature distribution of the gases along the barrel corresponding to shooting tests with solid propellant for grain size of 500–600 μm at initial temperatures from −60 °C to 60 °C are presented in Fig. 13. It's evident from this figure that temperature of combustion gases increases as the initial temperature gets higher. The firing tests with 10 shots were completed around 30 s. After that the barrel continued to cool down. When 10 shots were completed, the maximum inner surface temperature reached as high as 700 °C and rapidly fell down to 140 °C and finally the barrel was left for free cooling. As the cooling time increases temperatures of the inner and outer barrel surfaces get closer and for sufficiently high waiting time they become equal to each other.

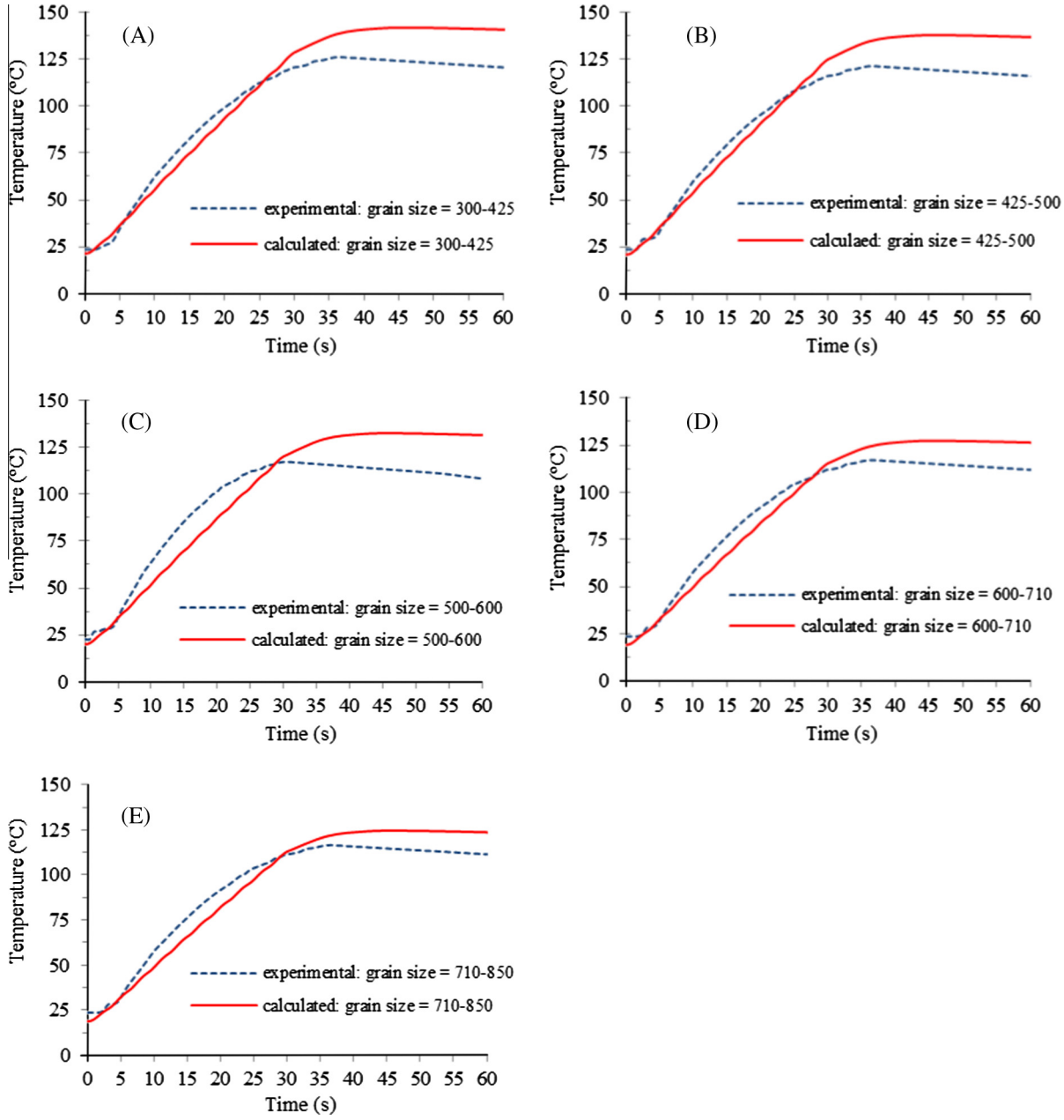


Fig. 12. Time dependent maximum temperature in the barrel corresponding to experimental–computational analysis of shooting tests at 20 °C with different propellant grain sizes: (A) 300–425 μm, (B) 425–500 μm, (C) 500–600 μm, (D) 600–710 μm, and (E) 710–850 μm.

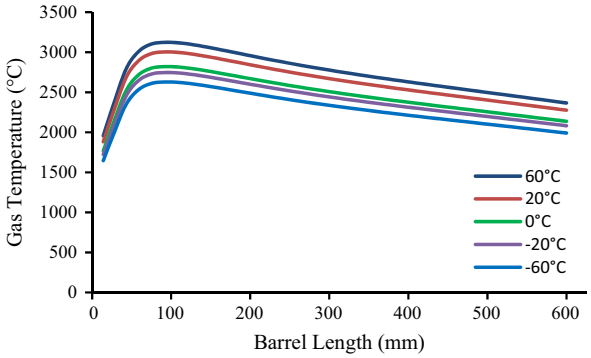


Fig. 13. The temperature distribution of gases along the barrel using solid propellant of 500–600 μm grain size at initial temperatures from −60 °C to 60 °C.

The maximum pressure in the barrel was measured by using piezoelectric transducers, and also strain gages were located at 24 points along the barrel which made it possible to determine the pressure distribution along the barrel. The pressure data along with the temperature calculations were utilized in the finite element analysis program ABAQUS to determine the stresses generated in the barrel as the bullet moved ahead. Equivalent maximum stresses along the barrel were calculated according to Von Mises theory. Fig. 14A reveals the effect of initial temperature of the propellant with grain size of 500–600 μm on the equivalent maximum stresses along the barrel. As it may be expected equivalent stresses increase depending on the increase in the initial temperature of the propellant which result in combustion gases with higher pressure and temperature. On the other hand, Fig. 14B displays the effect of grain size of the propellant, conditioned at 20 °C, on the equivalent stresses generated along the barrel. The propellant grain size obviously affects the interior ballistic parameters. Decreasing the grain size of the propellant increases the temperature and pressure of the combustion gases which then generates higher stresses in the barrel. Equivalent stresses decreased from the chamber to the muzzle as a consequence of higher pressure and temperature of the gases close to the chamber end.

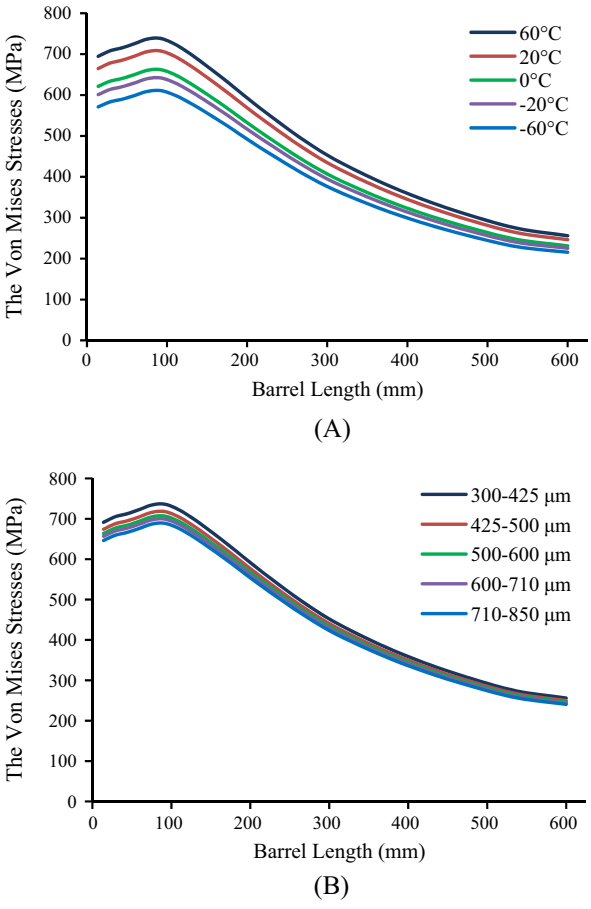


Fig. 14. The effect of (A) initial propellant temperature and (B) propellant grain size on the equivalent maximum stresses along the barrel.

Equivalent Von Mises stresses of the thermo-mechanically coupled model in ABAQUS conform to theoretically calculated stresses with high precision. Tables 3 and 4 summarize some of the interior ballistic parameters of the current study and make a comparison of experimental, numerical and analytical solutions on the basis of temperatures and stresses generated in the barrel. Table 3 presents a comparison of the maximum temperatures on the outer wall of the barrel for the computational–experimental study together with the comparison of maximum stresses on the inner wall for the com putational–theoretical study, employing solid propellants with grain size of 500–600 μm conditioned at different temperatures. Table 4 provides the same types of comparisons for solid propellants with various grain sizes which were all conditioned at 20 °C. Comparison of temperature and stress results corresponding to experimental and computational studies validates the thermo-mechanically coupled model in ABAQUS.

7. Conclusions

Variation of the grain size of the solid propellant as well as the initial temperature changes combustion characteristics which affect dynamic pressure and temperature. The interior ballistics parameters were comprehensively investigated employing experimental, numerical and analytical methods with a thermo-mechanical approach. A numerical model was developed and experimentally validated for the interior ballistics problem based on the propellant grain size at different conditioning temperatures. From the computational and experimental studies performed in this work, it was seen that as the initial temperature of the solid propellant increased or the grain size decreased, the inner and outer wall temperatures, internal pressure and bullet velocity increased. With all the tests, the stresses on the inner wall were the highest at the first shooting while the stresses were very low on the outer wall due to small thermal gradients. As the successive shots continued the thermal gradient on the inner wall decreased leading to lower stresses, whereas the thermal gradient on the outer wall increased leading to higher stresses.

The most important parameters to affect barrel behavior are thermal effects and stresses during successive shots. The current work included experimental and computational investigations of the effect of successive shots on temperature and thermal stresses on a barrel for periods of 3 s. It was seen that as the time between successive shots increased, inner and outer wall temperatures got closer to each other but the barrel heated up more and the left over gases in the barrel continued heating the material. At the first shooting, thermal stresses were the largest on the inner surface due to large temperature differences but as the successive shots occurred, the temperature difference lowered and thermal stresses on the inner wall decreased while thermal stresses on the outer wall increased. The thermal and stress analysis of interior ballistics problem was performed employing both finite element analysis program ABAQUS and analytical solution. Von Mises stresses calculated analytically along the barrel axis were perfectly conforming to the finite element solution. Overall, the simulations

Table 3
Effect of initial temperature of the propellant on the outer wall temperature and inner wall stress of the barrel based on computational, experimental and theoretical solutions.

		Initial temperature of the propellant				
		−60 °C	−20 °C	0 °C	20 °C	60 °C
Residence time of bullet (ms)		1.44	1.39	1.37	1.34	1.27
[Max. temperature on the outer wall (°C)]	Computational	110	120.6	125.9	132.5	145.5
	Experimental	99.7	109.6	114.1	117.4	136.4
[Max. stress on the inner wall (MPa)]	Computational	605.1	636.4	655.9	700.2	730.1
	Theoretical	611.3	641.9	662.4	707.9	738.8

Table 4
Effect of propellant grain size on the outer wall temperature and inner wall stress of the barrel based on computational, experimental and theoretical solutions.

		Grain size of the propellant (μm)				
		300–425	425–500	500–600	600–710	710–850
Residence time of bullet (ms)		1.27	1.30	1.34	1.37	1.42
[Max. temperature on the outer wall (°C)]	Computational	141	137.8	129.2	127.2	124.6
	Experimental	126.2	121.4	117.4	117.1	116.6
[Max. stress on the inner wall (MPa)]	Computational	727.8	709.2	698.2	691.1	680.5
	Theoretical	736.2	717.8	706.7	699.4	688.8

showed good agreement with the experiments. Experimental test procedure and experimental setup in such studies are very complex, expensive and require safety issues to be strictly applied. The developed model of this study can be used in other studies with the least experimental work to offer convenient solutions for various parametric studies.

Acknowledgements

The authors wish to thank to the Ministry of Industry of Turkey and to Turkish Mechanical and Chemical Industries (MKE) for financial support and technical cooperation.

References

[1] D.E. Carlucci, S.S. Jacobson, Ballistics Theory and Design of Guns and Ammunition, Taylor & Francis, Boca Raton, 2008.
[2] J. Corner, Theory of the Interior Ballistics of Guns, John Wiley & Sons Inc, New York, 1950.
[3] AMCP 706-247, Ammunition Series, Section 4: Design for Projection, Headquarters, U.S. Army Material Command, July 1964.
[4] G.P. Sutton, Rocket Propulsion Elements, seventh ed., USA, 2010 (ISBN 978-0-471-08024-5).
[5] N. Kubato, Propellant and Explosives, Germany, 2002 (ISBN: 3-527-30210-7).
[6] J.P. Agrawal, High Energy Materials, EY-VCH Verlag GmbH & Co. KGaA, Weinheim, 2010 (ISBN: 978-3-527-32610-5).
[7] E. Degirmenci, M.H. Dirikolu, A thermochemical approach for the determination of convection heat transfer coefficients in a gun barrel, Appl. Therm. Eng. 37 (2012) 275–279.
[8] H. Yaman, V. Celik, E. Degirmenci, Experimental investigation of the factors affecting the burning rate of solid rocket propellants, Fuel 115 (2014) 794–803.
[9] N. Yilmaz, B. Donaldson, W. Gill, Solid propellant burning rate from strand burner pressure measurement, Propell. Explos. Pyrot. 33 (2) (2008) 109–117.
[10] E. Degirmenci, Effects of grain size and temperature of double base solid propellants on internal ballistics performance, Fuel 146 (2015) 95–102.
[11] X.G. Wu, Q.L. Yan, X. Guo, X. FeiQi, X.J. Li, K.Q. Wang, Combustion efficiency and pyrochemical properties of micron-sized metal particles as the components of modified double-base propellant, Acta Astronaut. 1098–1112 (2011).
[12] L. Meda, G. Marra, L. Galfetti, F. Severini, L.D. Luca, Nano-aluminum as energetic material for rocket propellants, Mater. Sci. Eng. C 27 (2007) 1393–1396.
[13] S.J. Song, H.J. Kim, S.F. Ko, H.T. Oh, I.C. Kim, J.C. Yoo, J.Y. Jung, Measurement of solid propellant burning rates by analysis of ultrasonic full waveforms, J. Mech. Sci. Technol. 23 (2009) 1112–1117.
[14] H.L. Lee, Y.C. Yang, W.J. Chang, T.S. Wu, Estimation of heat flux and thermal stresses in multilayer gun barrel with thermal contact resistance, Appl. Math. Comput. 209 (2009) 211–221.
[15] B. Wu, G. Chen, W. Xia, Heat transfer in a 155 mm compound gun barrel with full length integral midwall cooling channels, Appl. Therm. Eng. 28 (2008) 881–888.
[16] D.Y. Chunga, N. Shin, M.Y. Oh, S.H. Yoo, S.H. Nam, Prediction of erosion from heat transfer measurements of 40 mm gun tubes, Wear 263 (2007) 246–250.
[17] S. Singh, P.K. Jain, R. Uddin, Analytical solution to transient heat conduction in polar coordinates with multiple layers in radial direction, Int. J. Therm. Sci. 47 (2008) 261–273.
[18] J.H. Underwood, G.N. Vigilante, C.P. Mulligan, Review of thermo-mechanical cracking and wear mechanisms in large caliber guns, Wear 263 (2007) 1616–1621.
[19] Y.A. Cengel, Heat Transfer: A Practical Approach, second ed., McGraw-Hill, 2003.
[20] A. Senturk, H. Isik, C. Evci, Thermo-mechanically coupled thermal and stress analysis of interior ballistics problem, Int. J. Therm. Sci. 104 (2016) 39–53.
[21] Y.Z. Chen, X.Y. Lin, Elastic analysis for thick cylinder and spherical pressure vessels made of functionally graded materials, Comput. Mater. Sci. 44 (2008) 581–587.
[22] Y. Orcan, Thermal stresses in a heat generating elastic-plastic cylinder with free ends, Int. J. Eng. Sci. 32 (1994) 883–898.
[23] AEP-97, Multi Calibre Manual of Proof and Inspection (M-C MOPI) for 5.56 mm, 7.62 mm, 9 mm and 12.7 mm Ammunition, NATO Standard, NATO Army Armaments Group (NAAG), NATO Standardization Agency (NSA).
[24] A.M. Law, W.D. Kelton, Simulation Modelling & Analysis, McGraw-Hill, Singapore, 1991.